Transonic Vortex Flows Past Delta Wings: Integral Equation Approach

Osama A. Kandil*
Old Dominion University, Norfolk, Virginia
and
E. Carson Yates Jr.†
NASA Langley Research Center, Hampton, Virginia

The steady full-potential equation is written in the form of Poisson's equation, and the solution of the velocity field is expressed in terms of an integral equation. The solution consists of a surface integral of vorticity distribution on the wing and its free-vortex sheets and a volume integral of source distribution within a volume around the wing and its free-vortex sheets. The solution is obtained through successive iteration cycles. The density gradient in the source distribution is computed by using a type-differencing scheme. The method is applied to delta wings, and the numerical examples show that a curved shock is captured on the suction side of the wing. It is attached to the lower surface of the leading-edge vortex but does not necessarily reach the wing surface. The present solution does not suffer from the numerical diffusion problem usually encountered with the finite-difference solutions of Euler equations.

Introduction

EFFICIENT aerodynamic design of fighter aircraft is still a challenge for computational aerodynamicists due to the various flow regimes encounted during fighter aircraft missions, such as during air-combat fighter missions and air-to-ground-strike missions. Throughout these missions, the flowfield may vary from essentially attached conditions to partly separated to fully separated conditions. In addition to these complex flow conditions, flow compressibility changes from low subsonic to supersonic Mach numbers during take-off, cruise, combat action, maneuvering, and landing. Bradley and Bhately[1] reviewed the status of computational methods with emphasis on fighter design applications. Their ratings of the existing computational techniques for fighter aircraft applications ranged from poor to fair, a status which urgently calls for improvements and development.

In the present paper, we deal with the problem of transonic vortex flows around highly swept wings—a key aerodynamic problem for the future development of super-maneuvering fighter aircraft. The procedure is an extension of the method of Ref. 2, in which we exploit the shock-capturing nature of the method through careful computation of the source distribution in the volume integral term that represents the full nonlinear compressibility in the flowfield.

Background

In this section, we briefly review the state-of-the-art of computational vortex flows for highly swept wings. For more extensive review, the reader should consult Refs. 3 and 50.

Integral-Equation Methods

In the low-speed regime, methods directly or indirectly obtained from the Green's function solution—integral-equation (IE) methods—have been developed for steady and unsteady flows. Existing methods of this type are the nonlinear discrete-vortex methods,[4-6] the doublet-panel methods,[7-11] the vortex-panel method,[12,13] and the velocity-potential-panel method.[14] The first-order flow compressibility has been accounted for by using the Prandtl-Glauert transformation based on the freestream Mach number.[15] For the upper subcritical flow regime, Kandil[2] has extended the nonlinear discrete-vortex method to solve the steady-state full-potential equation.

A survey of the literature reveals similar two-dimensional transonic flow methods that did not account for the vortex flow. These methods use the transonic small-perturbation (TSP) equation. Piers and Sloof[16] used the steady TSP equation for steady two-dimensional flows in conjunction with different forms of artificial viscosity terms, similar to those used in finite-difference methods, to capture shocks.

Tseng and Morino[17-19] used the TSP equation for three-dimensional steady and unsteady flows with prescribed wake. They have shown that the integral-equation formulation is of the shock-capturing type and that the contribution of the shock, as a surface of source distribution, is embedded in the volume-integral term representing the nonlinear compressibility. All that is needed to capture the shock is to compute accurately the derivatives of the volume integral term, which obviously requires a fine computational grid in the shock region to obtain good flow resolution. Although shock capturing was demonstrated, it apparently was not carried out using a fine computational grid due to the limited memory storage of the computer used.

A logical next step would be to vectorize the codes that employ the integral-equation method and make use of the large memory capacity and speed of parallel processors (CDC 205 or CRAY 2) to exploit the capability of this method in capturing shock waves accurately. One has to remember the power of this method in calculating free-vortex sheets. Moreover, the method is computationally economical since its accuracy depends on the evaluation of integrals rather than derivatives as in the finite-difference methods. With this method, the far-field boundary conditions are automatically satisfied and, hence, only a small-sized computational region is needed around the wing and its wake.

Presented as Paper 85-1582 at the AIAA Fluid Dynamics, Plasmadynamics and Lasers Conference, Cincinnati, OH, July 16-18, 1985; received Dec. 26, 1985; revision received March 31, 1986.

*Professor of Mechanical Engineering and Mechanics. Member AIAA.

†Chief Scientist, Load and Aeroelasticity Division. Associate Fellow AIAA.

Finite-Difference Methods

In developing finite-difference (FD) schemes to solve fluid dynamics problems, one has to evaluate carefully the stability of the scheme[20,21] through the analysis of truncation error terms of the so-called modified equation, which is the partial-differential equation actually solved by the FD scheme. Depending on the FD scheme used, the truncation error has two effects on the numerical solution: dissipation and dispersion. In the truncation error, even derivatives have a dissipative effect, while odd derivatives have a dispersive effect. For transonic flows, the dissipative effect smears the shock, while the dispersive effect produces oscillations in the solution that might blow up if safeguards are not added to the finite-difference scheme. The combined effect of dissipation and dispersion is a numerical diffusion that strongly affects regions of large vorticity.

In the period 1971-1980, steady and unsteady transonic flows without strong vortex flow[22-31] have been successfully solved using the TSP equation and the full-potential (FP) equation. Fully conservative relaxation (FCR) schemes and nonconservative relaxation (NCR) schemes have been developed for the TSP equation. The first NCR scheme was developed by Murman and Cole.[32] The scheme is of a mixed finite-difference type, whose results do not satisfy the shock-jump conditions. Later, the scheme was modified by Murman[33] to satisfy the proper jump conditions. Several schemes that use the FP equation in conservation-law form have been developed for steady and unsteady transonic flows.[26-31] Finite-volume schemes for the full-potential equation have also been developed.[34] Since the potential equation, in finite-difference solution, cannot treat flows that include nonplanar vortex wake, Murman and Stremel[35] used an adaptation of Baker's "cloud in cell" algorithm. Modeling the vortex wake as a group of discrete vortex points and tracking the vortex points in a Lagrangian frame of reference, they obtained the roll-up of vortex wake behind a large-aspect-ratio wing with a known spanwise lift distribution. Although the problem considered is simple compared to the complexity of transonic vortex flows around fighter aircraft, it demonstrated the feasibility of solving transonic vortex flow using the potential equation.

Before switching this review to Euler equations, it is worth mentioning that nonunique solutions of the conservative potential equation have been recently calculated for airfoils at moderate Mach number[36-38]—a very disturbing computational result. Salas and Gumbert[39] have shown that the problem appears universal because the isentropic-flow assumption underlying the potential-flow equation is violated as shock strength becomes finite. More recently, Fuglsang and Williams[40] have shown that the nonuniqueness can be eliminated by relatively minor modifications of potential-flow codes to account for entropy change across a shock of finite strength.

Shock waves with weak and moderate strength are typical for cruising flight of transport aircraft. For upper transonic range, where strong shocks exist and where entropy changes and vorticity production cannot be ignored, and for flows with distributed vorticity existing in the field, the potential equation simply breaks down unless these effects are carefully taken into account. Such flows are typical of fighter aircraft and helicopter blades as well.

Euler equations include the vorticity field and, in principle, should admit accurate solutions for rotational flows with shock waves. Very recently several methods that use the strong conservative form of the unsteady Euler equations have been developed to solve for steady and unsteady transonic flows.[41-48] For steady flows, the unsteady equations, which are hyperbolic, are solved in pseudo-time. In all these methods, with the exception of Ref. 47, different versions of the finite-volume method have been developed. Since the finite-volume method is approximately equivalent to a second-order-accurate central-difference scheme, explicit artificial dissipation is required to suppress wiggles in the neighborhood of shock waves due to the existence of odd derivatives in the truncation error. Although the addition of dissipative terms works very well in the shock region,[41] the combined effect of the artificial viscosity (dissipation effect) and the truncation error (dispersion effect) introduces diffusion of vorticity.[42-45] Therefore, solutions obtained by Euler equations have shown their capability of capturing vortical flow qualitatively but not quantitatively, generally due to the diffusion effect.

Recently, Roberts and Murman[46] and Sankar et al.,[47] in applying finite-difference computations to Euler equations for modeling vortex flows around helicopter blades, introduced a method to alleviate the numerical diffusion of the tip vortex. In these techniques, the velocity field in the Euler equation is split into two parts[49]: a known part and an unknown part. The known part is due to a tip vortex whose position, shape, and velocity field are known from a free-wake calculation procedure. The unknown part is considered an unknown perturbation velocity field about the known induced velocity field. The solution of the Euler equation yields the perturbation velocity field. Since the artificial viscosity term is applied only to the perturbation velocity field, the numerical diffusion will not affect the known induced velocity field. Such an approach reduces the need for higher-order finite-difference schemes or grid refinement and, hence, is computationally economical. Recently, the first author[50] developed a velocity-splitting technique for the Euler equation using a finite-volume scheme. This is the only economical computational procedure to solve the Euler equation for transonic vortex-dominated flows.

Formulation

Basic Approach of Subcritical Flows

The governing equations of the three-dimensional, steady, compressible, potential flow around a wing are given by

$$\Phi_{xx}+\Phi_{yy}+\Phi_{zz}=G \tag{1}$$

$$\rho=\{1+[(\gamma-1)/2]M_\infty^2(1-u^2-v^2-w^2)\}^{1/\gamma-1} \tag{2}$$

$$G=-(1/\rho)(\rho_x u+\rho_y v+\rho_z w) \tag{3}$$

where Φ is the total velocity potential, ρ the density, γ the ratio of specific heats, and M_∞ the freestream Mach number; u, v, and w are the velocity components of the total velocity $\bar{V}$, which is given by the Helmholtz decomposition

$$\bar{V}=\nabla\Phi+\bar{V}' \tag{4}$$

where $\bar{V}'$ is the solenoidal velocity due to the rotational flow. Note that Eq. (1) is obtained from the continuity equation using the solenoidal property of $\bar{V}'$, $\nabla\cdot\bar{V}'=0$.

The formal integral solution to Eq. (1) in terms of the velocity field is substituted into Eq. (4) to obtain the total velocity at any field point p,

$$\bar{V}_p(x,y,z)=\bar{e}_\infty+\frac{1}{4\pi}\iint_g\frac{q}{r^2}\bar{e}_r\,ds+\frac{1}{4\pi}\iint_g\frac{\bar{\omega}(\xi,\eta,\zeta)x\bar{r}}{r^3}\,ds$$
$$+\frac{1}{4\pi}\iint_w\frac{\bar{\omega}(\xi,\eta,\zeta)x\bar{r}}{r^3}\,ds+\frac{1}{4\pi}\iiint_v\frac{G(\xi,\eta,\zeta)}{r^2}\bar{e}_r\,dv \tag{5}$$

where $p(x,y,z)$ is a field point, $\bar{e}_\infty$ a unit vector in the freestream direction, q a surface source distribution, and $\bar{\omega}$ the vorticity vector; the subscripts g and w refer to the wing and free-vortex sheet surfaces, respectively, ξ, η, ζ are the coordinates of a source point, $r=[(x-\xi)^2+(y-\eta)^2+(z-\zeta)^2]^{1/2}$, and G is a source distribution in the flowfield. For a zero-thickness wing, the second term on the right-hand

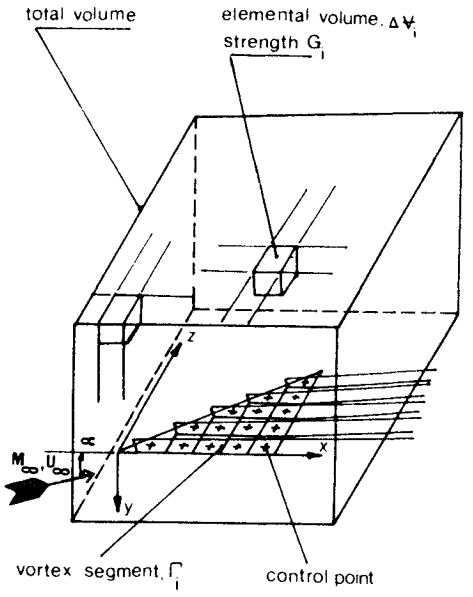

Fig. 1 Computational model for transonic-vortex flows using the integral equations.

side of Eq. (5) drops out. Note that the third term does not have to be a surface integral of vorticity since a surface integral of doublets can be used instead. The nonlinear compressibility effects are taken care of through the last term, the volume integral term. The fourth term represents the contribution to the velocity field due to the free-vortex sheets emanating from the wing separation lines. This term can also be read as $\bar{V}'$ since the vorticity in the field has been lumped into surface vorticity distributed on the free-vortex sheets. The last term is a volume integral term representing the linear and nonlinear compressibility in the flow.

Note that the integrand of the volume integral of Eq. (5) decreases rapidly with increasing distance from the wing/vortex system, not only because of the factor $(1/r^2)$ but also because G diminishes rapidly with increasing distance. Consequently, for computational purposes, the volume integral needs to be addressed only within the immediate vicinity of the wing/vortex system. For low to moderate subsonic Mach numbers, the compressibility terms in G reduce to $M_\infty^2 u_x$.

Basic Approach for Transonic Flows

For treating transonic flows, we consider two techniques—shock-capturing and shock-fitting techniques. Although these techniques are well known, we examine here their application to the integral-equation formulation of the free-vortex-flow problem.

In the shock-capturing technique, Eq. (5) is iteratively solved to satisfy the flow tangency condition on the wing, the Kutta condition along the separation edges, and the flow-tangency and no-pressure-jump conditions on the free-vortex sheets. The components of the density gradient ρ_x, ρ_y, and ρ_z of the nonlinear compressibility term G are calculated using a backward/central finite-difference scheme of the Murman-Cole type.[32] Backward-finite differencing is used at supersonic points, while central-finite differencing is used at subsonic points.

The reader should notice the difference between the present formulation and the formulation given by Tseng and Morino.[17] The present formulation is based on the velocity field in which the source term G contains first-order derivatives of density only, and the normal velocity is discontinuous across the shock. The Tseng and Morino formulation is based on the velocity potential in which the source term G contains first- and second-order derivatives of the

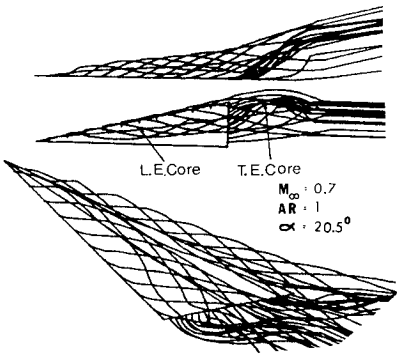

Fig. 2 Typical solution of the leading- and trailing-edge free-vortex lines.

velocity potential and the velocity potential is continuous across the shock. The present formulation has two advantages over the velocity-potential formulation: 1) only first-order derivatives need to be calculated by finite differencing, and 2) one does not need to calculate derivatives of the velocity potential in order to detect the shock formation since the velocity field is calculated directly in the present formulation.

An alternative shock-capturing technique of future interest is to use an artificial density,[51] along with central differencing, everywhere for calculating the density derivatives.

In the shock-fitting technique, the contribution of the shock to the velocity field is represented by an explicit surface-integral term of source distribution in Eq. (5), which then becomes (for zero thickness wing)

$$\bar{V}_p(x,y,z) = \bar{e}_\infty + \iint_{g,w} \frac{\bar{\omega}(\xi,\eta,\zeta)x\bar{r}}{r^3}\,ds + \frac{1}{4\pi}\iiint_V \frac{G(\xi,\eta,\zeta)}{r^2}\,\bar{e}_r\,dV + \frac{1}{4\pi}\iint_k \frac{q(\xi,\eta,\zeta)}{r^2}\,\bar{e}_r\,ds \quad (6)$$

where the subscript k refers to the shock surface, and the shock strength q is given by the normal-velocity increment across it. Thus,

$$q = V_{1n} - V_{2n} \quad (7)$$

The conditions behind the shock are determined by using the Rankine-Hugoniot relation

$$\frac{V_{1n}}{V_{2n}} = \frac{\rho_2}{\rho_1} = \frac{(\gamma+1)M_{1n}^2}{(\gamma-1)M_{1n}^2+2} \quad (8)$$

where the subscript n refers to the normal direction to the shock surface, and the subscripts 1 and 2 refer to the supersonic and subsonic sides of the shock, respectively. Solving Eq. (8) for V_{2n} and substituting the result into Eq. (7), we obtain an expression for q in terms of V_{1n} and M_{1n}

$$q = \frac{2V_{1n}}{\gamma+1}\left(1 - \frac{1}{M_{1n}^2}\right) \quad (9)$$

The density behind the shock ρ_2 is obtained from Eqs. (8) and (2)

$$\rho_2 = \frac{(\gamma+1)M_{1n}^2}{(\gamma-1)M_{1n}^2+2}\left[1 + \frac{\gamma-1}{2}M_\infty^2(1-u_1^2-v_1^2-w_1^2)\right]^{1/(\gamma-1)} \quad (10)$$

where u_1, v_1, and w_1 are the velocity components ahead of the shock. Equations (6), (9), and (10) are the basic equa-

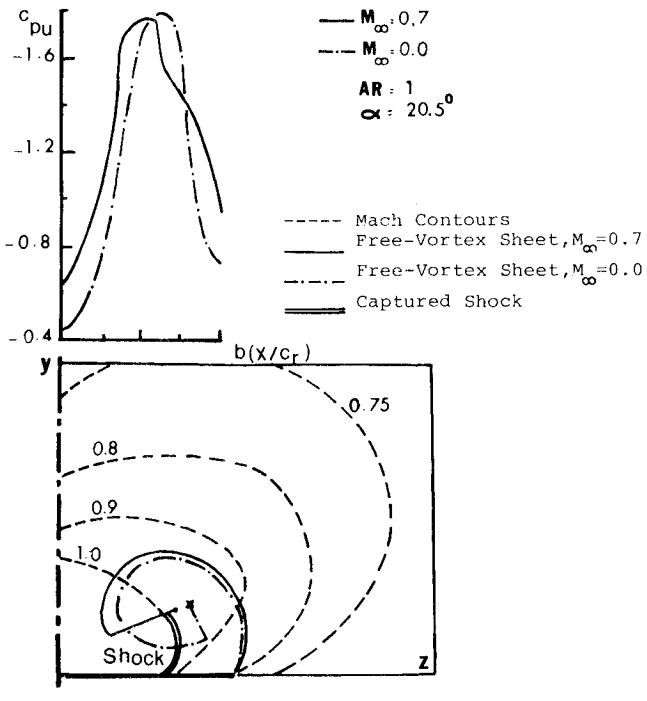

Fig. 3 Spanwise pressure variation and details of the flow in a cross-flow plane at $x/C_r = 0.5$.

tions for the shock-fitting technique. Such a technique would sharpen the shock without requiring local grid refinement.

It should be emphasized here that it is not essential to treat the shock contribution explicitly as a separate surface-integral term as given in Eq. (6), since the volume integral itself implicitly includes the shock surface contribution. This can be shown by writing Eq. (1) in the form

$$\nabla \cdot \bar{V} = G \tag{11}$$

Integrating Eq. (1) over an infinitesimal volume around an infinitesimal area of shock surface and applying the divergence theorem, one obtains

$$V_{1n} - V_{2n} = G\epsilon \tag{12}$$

where ϵ is an infinitesimal thickness normal to the shock surface. Equation (12) is equivalent to Eq. (7) if $G\epsilon = q$ and, hence, the volume-integral term in Eq. (6) reduces around the shock to the surface-integral term representing the shock surface in the same equation. This result has been shown also by Tseng and Morino.[17] Thus, one concludes that if the computational grid in the shock region is refined enough, the shock contribution need not be treated explicitly and Eq. (5) is able to capture the shock. The relative benefit of shock fitting for the free-vortex problem should be examined further, however, in terms of the computational cost of grid refinement vs the cost of explicit shock treatment.

Solution Procedure

In this paper, we implement the shock-capturing technique only. The solution procedure consists of two computational steps: 1) computation using the linear (Prandtl-Glauert) compressibility and 2) computation using the nonlinear (full-potential) compressibility. In the first step, flow compressibility is introduced as $G = M_\infty^2 u_x$ while in the second step, flow compressibility is calculated by Eq. (3). The details of the two steps follow:

Computation Using the Linear Compressibility

With $G = M_\infty^2 u_x$, Eq. (1) reduces to Laplace's equation in the equivalent incompressible space

$$\Phi_{x'x'} + \Phi_{y'y'} + \Phi_{z'z'} = 0 \tag{13}$$

where

$$x' = x/\beta, \qquad y' = y, \qquad z' = z, \qquad \beta = (1 - M_\infty^2)^{1/2} \tag{14}$$

The problem given by Eq. (13) and the corresponding wing and free-vortex sheet boundary conditions is solved iteratively to satisfy the boundary conditions (wake-iteration cycles) by using the modified nonlinear discrete-vortex (MNDV) method.[6] In this method, the paths of free-vortex lines emanating from the leading and trailing edges are calculated as part of the solution, and ultimately downstream they are fed into separate concentrated vortex cores, respectively. The results of this step are the circulation distribution and the shape of free-vortex lines, along with the vortex cores. Next, a rectangular three-dimensional grid is generated within a finite volume around the wing and its free-vortex lines (Fig. 1). Initial values of the volume source distribution are calculated by

$$G(i+\tfrac{1}{2}, j+\tfrac{1}{2}, k+\tfrac{1}{2}) = M_\infty^2 u_x(i+\tfrac{1}{2}, j+\tfrac{1}{2}, k+\tfrac{1}{2}) \tag{15}$$

where $i+\frac{1}{2}, j+\frac{1}{2}, k+\frac{1}{2}$ refer to the centroid of an elemental source volume $\Delta\forall$, and u_x is the sum of the x derivatives of the x components of velocity induced at the centroid by all the vortex elements and by the source elements in the flowfield. In these calculations, the source strength is taken constant within the elemental volume (equal to the value at the centroid). Before switching to the nonlinear compressibility step, a wake-iteration cycle is executed.

Computation Using the Nonlinear Compressibility

With the free-vortex lines fixed, the nonlinear flow compressibility is calculated by using Eqs. (2) and (3) in the form

$$\rho(i+\tfrac{1}{2}, j+\tfrac{1}{2}, k+\tfrac{1}{2}) = \{1 + [(\gamma-1)/2] M_\infty^2 \times [1 - u^2(i+\tfrac{1}{2}, j+\tfrac{1}{2}, k+\tfrac{1}{2}) - v^2(i+\tfrac{1}{2}, j+\tfrac{1}{2}, k+\tfrac{1}{2}) - w^2(i+\tfrac{1}{2}, j+\tfrac{1}{2}, k+\tfrac{1}{2})]\}^{1/\gamma-1} \tag{16}$$

$$G(i+\tfrac{1}{2}, j+\tfrac{1}{2}, k+\tfrac{1}{2}) = -[(1/\rho)(\rho_x u + \rho_y v + \rho_z w)]_{(i+\frac{1}{2}, j+\frac{1}{2}, k+\frac{1}{2})} \tag{17}$$

where u, v, w are the components of total velocity, including the freestream velocity and the velocity induced by all the vortex lines and elemental source volumes. The components of the density gradient, ρ_x, ρ_y, and ρ_z, are calculated using central differencing at subsonic points and backward differencing at supersonic points. For example, the x derivative of the density is obtained by

$$\rho_x(i+\tfrac{1}{2}, j+\tfrac{1}{2}, k+\tfrac{1}{2}) = \frac{\rho(i, j+\tfrac{1}{2}, k+\tfrac{1}{2}) - \rho(i+1, j+\tfrac{1}{2}, k+\tfrac{1}{2})}{x(i, j+\tfrac{1}{2}, k+\tfrac{1}{2}) - x(i+1, j+\tfrac{1}{2}, k+\tfrac{1}{2})}$$

$$\text{for } M(1+\tfrac{1}{2}, j+\tfrac{1}{2}, k+\tfrac{1}{2}) < 1 \tag{18}$$

or

$$\rho_x(i+\tfrac{1}{2}, j+\tfrac{1}{2}, k+\tfrac{1}{2}) = \frac{\rho(i, j+\tfrac{1}{2}, k+\tfrac{1}{2}) - \rho(i-1, j+\tfrac{1}{2}, k+\tfrac{1}{2})}{x(i, j+\tfrac{1}{2}, k+\tfrac{1}{2}) - x(i-1, j+\tfrac{1}{2}, k+\tfrac{1}{2})}$$

$$\text{for } M(i+\tfrac{1}{2}, j+\tfrac{1}{2}, k+\tfrac{1}{2}) > 1 \tag{19}$$

This step is called the compressibility-iteration cycle.

Next, $G(i+\frac{1}{2}, j+\frac{1}{2}, k+\frac{1}{2})$ values are kept constant while a wake-iteration cycle is executed. The compressibility- and wake-iteration cycles are successively executed until the circulation and source distributions converge. The pressure coefficient is calculated by using the full Bernoulli equation

$$p=\frac{2}{\gamma M_\infty^2}\left\{\left[1+\frac{\gamma+1}{2}M_\infty^2(1-V^2)\right]^{\gamma/(\gamma-1)}-1\right\} \quad (20)$$

where

$$\bar{V}=\bar{e}_\infty+\bar{V}_G+\bar{V}_{\Gamma g}+\bar{V}_{\Gamma w} \quad (21)$$

where $\bar{V}_G$ is the velocity induced by the source distribution,[2] $\bar{V}_{\Gamma g}$ the velocity induced by bound vortices, and $\bar{V}_{\Gamma w}$ the velocity induced by the free vortices. Note that when calculating the pressure on the surface, the self-induced velocity must be treated explicitly.

Numerical Examples

A scalar program has been developed to implement the solution procedure of the shock-capturing technique. To prove the concept and verify the algorithm, the code is applied to delta wings at large angles of attack and high subsonic Mach numbers.

The first numerical example is an application to a delta wing with aspect ratio AR of 1, angle of attack α of 20.5 deg, and freestream Mach number M_∞ of 0.7. For this case, a 10×10 bound-vortex lattice is used on the wing, and the free-vortex sheet computation is carried out up to 0.6 of the wing root chord (C_r) behind the wing trailing edge. The rectangular grid around the wing and its free-vortex sheets consists of $17\times13\times13$ grid points and step sizes of $1\times0.25\times0.25$ in the x, y, and z directions, respectively. Convergence has been achieved after 10 wake-iteration cycles and 5 compressibility-iteration cycles, which took about 62 min of CPU time on the CYBER-175. It should be emphasized here that this code is a proof of concept code, and no attempt has been made to enhance its efficiency. Because of the exploratory nature of the problem, the computations have been carried out with discontinuous runs, each of which took approximately 12 min.

Figure 2 shows the computed leading- and trailing-edge free-vortex lines and inviscid vortex cores in two- and three-dimensional views. Figures 3-5 show details of the flow in cross-flow planes at the chord stations 0.5, 0.7, and 0.86. In each figure, we show the local Mach number contours, the captured shock wave, the leading-edge vortex sheet and its vortex core along with those of the incompressible flow, and the spanwise variation of pressure on the upper surface of the wing along with that of the incompressible flow. It is evident that the captured shock has a curved shape, is attached to the vortex sheet, is located almost at the spanwise location of the leading-edge vortex core, and does not necessarily reach to the leeward side of the wing. In these preliminary calculations, it is shown that for forward cross-flow planes, the foot of the shock is attached to the feeding vortex cut, which is a computational artifice. This can be cured by considering an additional half-turn of the free-vortex lines before they are dumped in the vortex core. Moreover, it is seen that the vortex core of the transonic flow is nearer the wing surface than that of the incompressible flow. The upper-surface pressure distribution also shows the existence of the shock. Although no attempt has yet been carried out to refine the grid or fit the shock, the computed results clearly show the shock-capturing nature of the integral-equation approach.

Figure 6 shows the flow directions, the leading- and trailing-edge vortex sheets and their vortex cores as well (the trailing-edge core forms at almost $0.25C_r$ behind the trailing edge) in cross-flow planes that are normal to the wind direction (note that $\hat{o}\bar{x}$ is parallel to $\bar{U}_\infty$). The shock disappears at almost $0.1C_r$ behind the trailing edge.

In the second numerical example, we consider a delta wing with an aspect ratio of 1.5, an angle of attack of 15 deg, and a freestream Mach number of 0.8. This case has also been considered by Rizzi in Refs. 52 and 53 through a finite-volume Euler code that uses an 0-0 type mesh consisting of $65\times30\times42$ and $161\times49\times81$, respectively. Figure 7 shows the computed leading- and trailing-edge free-vortex lines and inviscid vortex cores in two- and three-dimensional views.

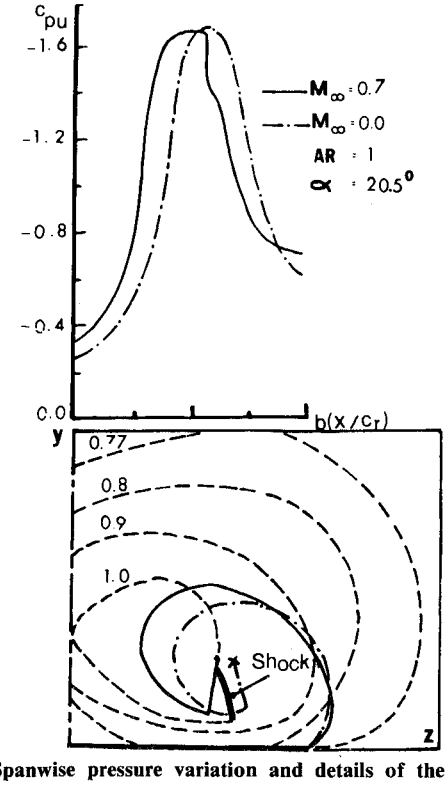

Fig. 4 Spanwise pressure variation and details of the flow in a cross-flow plane at $x/C_r=0.7$.

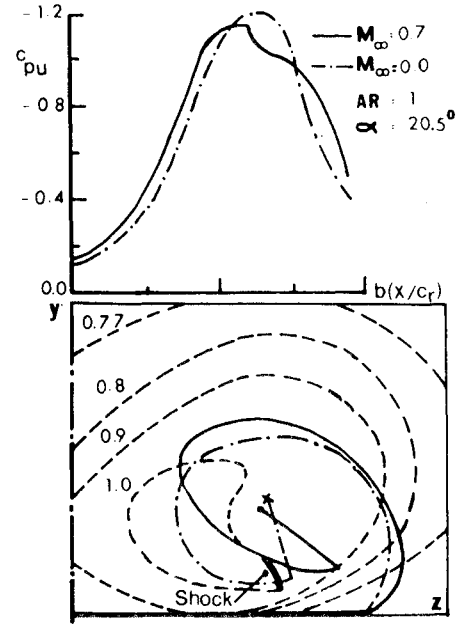

Fig. 5 Spanwise pressure variation and details of the flow in a cross-flow plane at $x/C_r=0.86$.

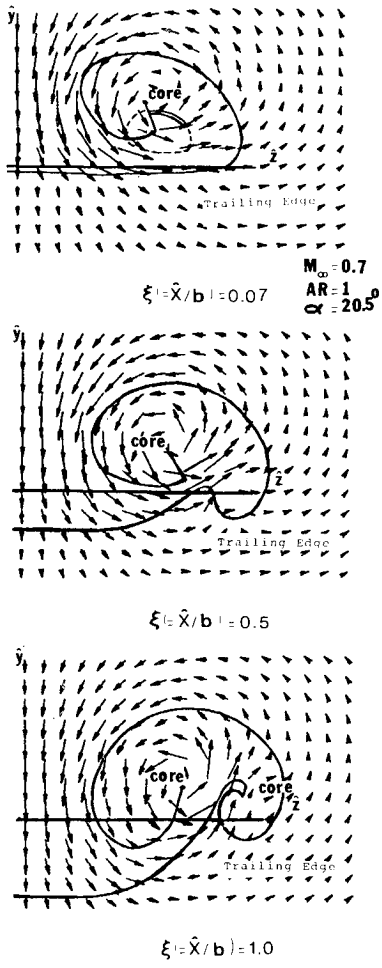

Fig. 6 Flow directions and free-vortex sheet behind the trailing edge in cross-flow planes normal to the wind direction.

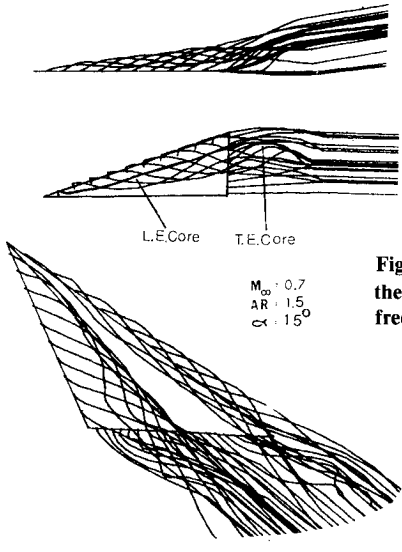

Fig. 7 Typical solution of the leading- and trailing-edge free-vortex lines.

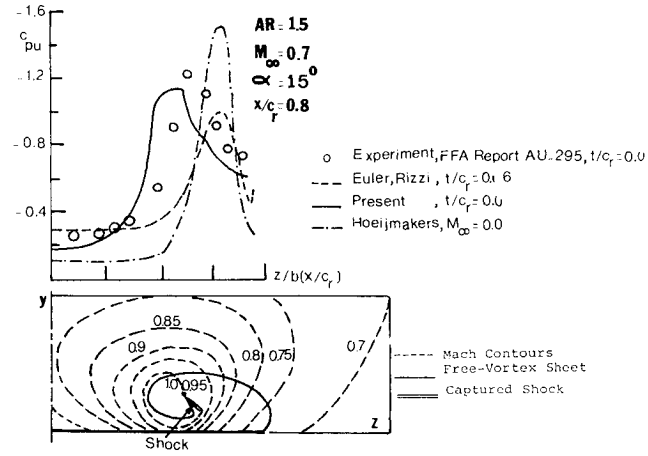

Fig. 8 Spanwise pressure variation and details of the flow in a cross-flow plane at $x/C_r = 0.86$.

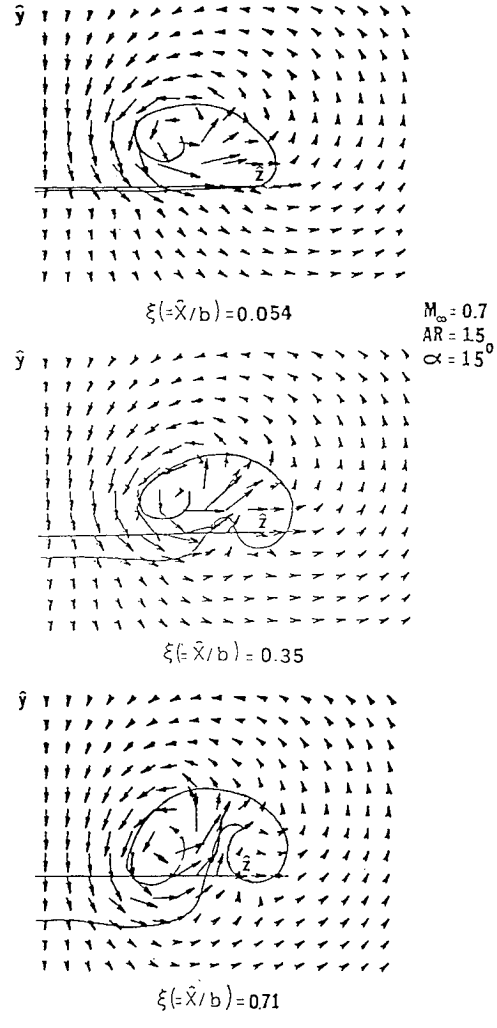

Fig. 9 Flow directions and free-vortex sheet behind the trailing edge in cross-flow planes normal to the wind direction.

Figure 8 diagrams the spanwise surface pressure variation and details of the flow in a cross-flow plane at a chord station of 0.8. On the same figure, we compare the surface pressure computed by the present method with those computed by Rizzi[52] and Hoeijmakers[11] ($M_\infty = 0.0$). We also include the experimental data used by Rizzi.[52] It is obvious that the present method compares favorably with the experimental data while the Euler solver[52] substantially underpredicts the peak pressure and mispredicts the location of the leading-edge vortex core. Even with the recent fine grid,[53] one million grid points, prediction of the leading-edge vortex core did not improve. Similar disappointing results were reported earlier by Raj and Sikora.[45] There are two reasons for such disappointing results with the existing Euler codes. The first reason is the diffusive effect of the artificial dissipation terms on the vortex-dominated regions; the second reason is the lack of a Kutta condition and, hence, the absence of a unique mechanism for the vorticity shedding along the separation edges, since we are dealing with inviscid equations.

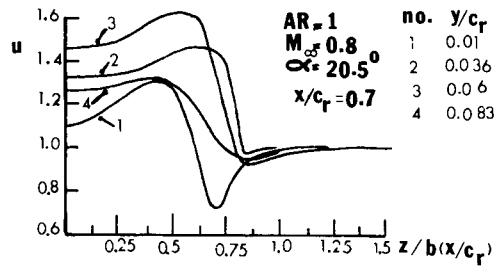

Fig. 10 Spanwise variation of the axial velocity at different heights above the leeward side.

In a recent paper, Newsome and Thomas[54] showed that with central differencing using Euler equations on a coarse grid, a vortex was captured. Using a fine grid, the vortex disappeared and, as they concluded, this vortex is due entirely to numerical error.

Figure 9 shows the flow directions behind the trailing edge in cross-flow planes normal to the wind direction.

Figure 10 shows the spanwise variation of the axial velocity in the flowfield through the shock at $x/C_r = 0.7$ for a delta wing of aspect ratio 1, angle of attack 20.5 deg, and freestream Mach number 0.8. It is obvious that a curved shock exists and is captured.

All the computed results are in agreement with most of the conclusions of the experimental work of Ref. 55. In particular, a shock has been captured under the roll-up vortex sheet at almost the same spanwise location as that of the leading-edge vortex core. Moreover, the vortex core in the compressible flow moves closer to the wing surface than that of the incompressible flow. However, the conclusions of the experimental work[55] do not refer to the possibility that the shock may not reach the leeward side of the wing near the trailing edge. This should be physically logical: the shock gets weaker near the leeward side of the wing because it is further away from the leading-edge vortex core. Moreover, the vortex-core path moves higher above the leeward side as it approaches the trailing edge.

Conclusion

The numerical results of the integral-equation approach for the transonic vortex flow problem clearly show that the integral-equation solution is able to capture the shock. The captured shock is of curved shape, its foot is attached to the lower surface of the leading-edge vortex sheet, it does not necessarily reach to the leeward side of the wing, and it is located almost at the spanwise location of the leading-edge vortex core. In the cases considered here, the shock was found to disappear at almost 10% of the root chord behind the trailing edge. The computed results of the compressible flow, compared to those of the incompressible flows, show that the leading-edge vortex core moves a little inboard from the leading edge and a little downward nearer the suction side. The present velocity-field formulation is more advantageous than the earlier velocity-potential formulations for both the shock and vortex-sheet calculations.

It should be pointed out that no attempt has been made to show the convergence of the solution vs the number of grid points of the finite volume. More work is still needed to prove this point and, moreover, to sharpen the shock, either by refining the grid in the shock region or by fitting the shock while using a relatively coarse grid. In addition, the MNDV method should be replaced by the NHV method,[13] and an additional half-turn of the leading-edge vortex system should be considered to cure the problem of having the foot of the shock attached to the feeding vortex cut in the forward cross-flow planes. Finally, the merits of monotone differencing should be considered instead of classical differencing. In addition to these improvements, the code should be transferred to a parallel processor.

Acknowledgments

This research work is supported by NASA Langley Research Center under Grant No. NAG-1-591.

References

[1]Bradley, R. G. and Bhateley, I. C., "Computational Aerodynamic Design of Fighter Aircraft—Progress and Pitfalls," AIAA Paper 83-2063, Aug. 1983.

[2]Kandil, O. A., "Computational Technique for Three-Dimensional Compressible Flow Past Wings at High Angles of Attack," AIAA Paper 83-2078, Aug. 1983, also in the *Journal of Aircraft*, Vol. 22, Sept. 1985, pp. 750-755.

[3]Kandil, O. A. and Yates, E. C. Jr., "Computation of Transonic Vortex Flows Past Delta Wings-Integral Equation Approach," AIAA Paper 85-1582, July 1985.

[4]Kandil, O. A., Mook, D. T., and Nayfeh, A. H., "Nonlinear Prediction of the Aerodynamic Loads on Lifting Surfaces," *Journal of Aircraft*, Vol. 12, Jan. 1976, pp. 22-28.

[5]Kandil, O. A., Mook, D. T., and Nayfeh, A. H., "A Numerical Technique for Computing Subsonic Flow Past Three-Dimensional Canard-Wing Configurations with Edge Separation," AIAA Paper 79-0282, Jan. 1979.

[6]Kandil, O. A. and Balakrishnan, L., "Recent Improvements in the Predictions of the Leading- and Trailing-Edge Vortex Cores of Delta Wings," AIAA Paper 81-1263, June 1981.

[7]Johnson, F. T., Tinoco, E. N., Lu, P., and Epton, M. A., "Recent Advances in the Solution of Three-Dimensional Flows Over Wings with Leading-Edge Vortex Separation," AIAA Paper 79-0282, Jan. 1977.

[8]Hoeijmakers, H. W. M. and Vaatstra, W., "A Higher-Order Panel Method Applied to Vortex Sheet Roll-Up," AIAA Paper 82-0096, Jan. 1982.

[9]Luckring, J. M., Schoonover, W. E. Jr., and Frank, N. T., "Recent Advances in Applying Free Vortex Sheet Theory for the Estimation of Vortex Flow Aerodynamics," AIAA Paper 82-0095, 1982.

[10]Lamar, J. E. and Campbell, J. F., "Recent Studies at NASA-Langley of Vortical Flows Interacting with Neighboring Surfaces," AGARD CP 342, April 1983.

[11]Hoeijmakers, H. M., "Computational Vortex Flow Aerodynamic," AGARD CP 342, April 1983.

[12]Kandil, O. A., Chu, L. C., and Yates, E. C. Jr., "Hybrid Vortex Method for Lifting Surfaces with Free Vortex Flow," AIAA Paper 80-0070, Jan. 1980.

[13]Kandil, O. A., Chu, L., and Turead, T., "A Nonlinear Hybrid Vortex Method for Wings at Large Angle of Attack," AIAA Paper 82-0351, Jan. 1982; also *AIAA Journal*, Vol. 22, March 1984.

[14]Suciu, E. O. and Morino, L., "Nonlinear Steady Incompressible Lifting Surface Analysis with Wake Roll-Up," *AIAA Journal*, Vol. 15, Jan. 1977, pp. 54-58.

[15]Kandil, O. A., Mook, D. T., and Nayfeh, A. H., "Subsonic Loads on Wings Having Sharp Leading-Edges and Tips," *Journal of Aircraft*, Vol. 13, Jan. 1976, pp. 62-63.

[16]Piers, W. J. and Sloof, J. W., "Calculation of Transonic Flow by Means of a Shock-Capturing Field Panel Method," AIAA Paper 79-1459, July 1979.

[17]Tseng, K. and Morino, L., "Nonlinear Green's Function Method for Unsteady Transonic Flows," *Progress in Aeronautics and Astronautics: Transonic Aerodynamics*, Vol. 81, edited by D. Nixon, AIAA, New York, 1982, pp. 565-603.

[18]Morino, L. and Tseng, K., "Time-Domain Green's Function Method for Three-Dimensional Nonlinear Subsonic Flows," AIAA Paper 78-1204, July 1978.

[19]Tseng, K., "Nonlinear Green's Function Method for Transonic Potential Flow," Ph.D. Dissertation, Boston University, 1983.

[20]Anderson, D. A., Tannehill, J. C., and Pletcher, R. H., *Computational Fluid Mechanics and Heat Transfer*, McGraw-Hill Book Co., New York, 1984.

[21]Peyret, R. and Taylor, T. D., *Computational Methods in Fluid Flow*, Springer-Verlag, New York, 1983.

[22]Spreiter, J. R., "Transonic Aerodynamics—History and Statement of the Problem," *Progress in Aeronautics and Astronautics: Transonic Aerodynamics*, Vol. 81, edited by D. Nixon, AIAA, New York, 1982, pp. 3-79.

[23]Jameson, A., "Transonic Flow Calculations," *Numerical Methods in Fluid Dynamics*, Hemisphere Publishing Corp., New York, 1978, pp. 1-87.

[24]Ballhaus, W. F., "Some Recent Progress in Transonic Flow Computations," *Numerical Methods in Fluid Dynamics*, Hemisphere Publishing Corp., New York, 1978, pp. 155-234.

[25]Schmidt, W., "Progress in Transonic Flow Computation," *Numerical Methods in Fluid Dynamics*, Hemisphere Publishing Corp., New York, 1978, pp. 299-338.

[26]Holst, T. L., "A Fast, Conservation Algorithm for Solving the Transonic Full-Potential Equations," *Proceedings of AIAA 4th Computational Fluid Dynamics Conference*, July 1979.

[27]Borland, C., Rizzetta, D., and Yoshihara, H., "Numerical Solution of Three-Dimensional Unsteady Transonic Flow Over Swept Wings," AIAA Paper 80-1369, July 1980.

[28]Sankar, J. B., Malone, N. L., and Tassa, Y., "An Implicit Conservative Algorithm for the Calculation of Transonic Flow Over Wing/Body Combinations," AIAA Paper 81-1016, June 1981.

[29]Chipman, R. and Jameson, A., "Fully Conservative Numerical Solutions for Unsteady Irrotational Transonic Flow about Airfoil," AIAA Paper 79-1555, 1979.

[30]Goorjian, P. M., "Computations of Unsteady Transonic Flow Governed by the Conservative Full Potential Equations Using an Alternating Direction Implicit Algorithm," NASA CR-152274, 1979.

[31]Steger, J. L. and Caradonna, F. X., "A Conservative Implicity Finite Difference Algorithm for the Unsteady Transonic Full Potential Equation," AIAA Paper 80-1368, 1980.

[32]Murman, E. M. and Cole, J. D., "Calculation of Plane Steady Transonic Flows," *AIAA Journal*, Vol. 9, Jan. 1971, pp. 114-121.

[33]Murman, E. M., "Transonic Aerodynamics," AIAA Professional Study Series, AIAA, New York, 1975.

[34]Caughey, D. A. and Jameson, A., "Recent Progress in Finite-Volume Calculations for Wing-Fuselage Combination," AIAA Paper 79-1513, 1979.

[35]Murman, E. M. and Stremel, P. M., "A Vortex Wake Capturing Method for Potential Flow Calculations," AIAA Paper 82-0947, June 1982.

[36]Rizzi, A. and Viviand, H. (eds.), "Numerical Methods for Computation of Inviscid Transonic Flow with Shocks," *Proceedings of GAMM Workshop, Stockholm,* 1979, Viewveg Verlag, Brunswick, Germany, 1981.

[37]Steinhoff, J. and Jameson, A., "Multiple Solutions of the Transonic Potential Flow Equation," AIAA Paper 81-1019, June 1981.

[38]Salas, M. D., Jameson, A., and Melnik, R. E., "A Comparative Study of the Nonuniqueness Problem of the Potential Equation," AIAA Paper 83-1888, July 1983.

[39]Salas, M. D. and Gumber, C. R., "Breakdown of the Conservative Potential Equation," *Symposium on Aerodynamics*, NASA Langley Research Center, Vol. 1, April, 1985, pp. 4.3-4.53.

[40]Fuglsang, D. F. and Williams, M. H., "Non-Isentropic Unsteady Transonic Small Disturbance Theory," AIAA Paper 85-0600, April, 1985.

[41]Jameson, A., Schmidt, W., and Turkel, E., "Numerical Solutions of the Euler Equations by Finite Volume Methods Using Runge-Kutta Time-Stepping Schemes, AIAA Paper 81-1259, June 1981.

[42]Erikson, L. E. and Rizzi, A., "Computation of Vortex Flow Around Wings Using the Euler Equations," *Notes on Numerical Fluid Mechanics*, Vol. 5, Nov. 1981, pp. 87-105.

[43]Rizzi, A., "Mesh Influence on Vortex Shedding in Inviscid Flow Computations," *Recent Contributions to Fluid Mechanics*, edited by W. Haase, Springer-Verlag, New York, 1982, pp. 213-221.

[44]Krause, E., Shi, X.-G., and Hartwich, P.-M., "Computation of Leading Edge Vortices," AIAA Paper 83-1907, July 1983.

[45]Raj, P. and Sikora, J. S., "Free-Vortex Flows: Recent Encounters with an Euler Code," AIAA Paper 84-0135, Jan. 1984.

[46]Roberts, W. T. and Murman, E. M., "Solution Method for a Hovering Helicopter Rotor Using the Euler Equations," AIAA Paper 85-0436, Jan. 1985.

[47]Sankar, N. L., Wake, B. E., and Lekoudis, S. G., "Solution of the Unsteady Euler Equations for Fixed and Rotor Wing Configurations," AIAA Paper 85-0120, Jan. 1985.

[48]Deese, J. E., "Split-Flux-Vector Solutions of the Euler Equations for Three-Dimensional Configurations," AIAA Paper 85-0434, Jan. 1985.

[49]Srinivasan, G. R., McCroskey, W. J., and Kutler, P., "Numerical Solution of the Interaction of a Vortex with a Stationary Airfoil in Transonic Flow," AIAA Paper 84-0254, Jan. 1984.

[50]Kandil, O. A., "Transonic Vortex Flow of Lifting Surfaces with Shock and Vortex-Sheet Fittings," *XVII Symposium on Advanced Problems and Methods in Fluid Mechanics*, Polish Academy of Sciences, Sobieszewo, Poland, Sept. 1985, pp. 77-78.

[51]Hafez, M., South, J., and Murman, E., "Artificial Compressibility Methods for Numerical Solution of Transonic Full Potential Equation," *AIAA Journal*, Vol. 17, Aug. 1979, pp. 838-844.

[52]Rizzi, A. and Eriksson, L. E., "Numerical Solutions of the Euler Equations Simulating Vortex Flows Around Wings," AGARD CP 342, April 1983, pp. 21.1-21.14.

[53]Rizzi, A., "Three-Dimensional Solutions to the Euler Equations with One Million Grid Points," *AIAA Journal*, Vol. 23, Dec. 1985, pp. 1986-1987.

[54]Newsome, R. W. and Thomas, J. L., "Computation of Leading-Edge Vortex Flows," Presented at the Vortex Flow Aerodynamics Conference, NASA Langley Research Center, Oct. 1985.

[55]Vorropoulos, G. and Wendt, J. F., "Laser Velocimetry Study of Compressible Effects on the Flow Field of a Delta Wing," AGARD CP 342, April 1983.